

---

# Average gradient outer product as a mechanism for deep neural collapse

---

Daniel Beaglehole<sup>\*1</sup> Peter Súkeník<sup>\*2</sup> Marco Mondelli<sup>2</sup> Mikhail Belkin<sup>1</sup>

## Abstract

Deep Neural Collapse (DNC) refers to the surprisingly rigid structure of the data representations in the final layers of Deep Neural Networks (DNNs). Though the phenomenon has been measured in a wide variety of settings, its emergence is only partially understood. In this work, we provide substantial evidence that DNC formation occurs primarily through deep feature learning with the average gradient outer product (AGOP). This takes a step further compared to efforts that explain neural collapse via feature-agnostic approaches, such as the unconstrained features model. We proceed by providing evidence that the right singular vectors and values of the weights are responsible for the majority of within-class variability collapse in DNNs. As shown in recent work, this singular structure is highly correlated with that of the AGOP. We then establish experimentally and theoretically that AGOP induces neural collapse in a randomly initialized neural network. In particular, we demonstrate that Deep Recursive Feature Machines, a method originally introduced as an abstraction for AGOP feature learning in convolutional neural networks, exhibits DNC.

## 1. Introduction

How Deep Neural Networks (DNNs) learn a transformation of the data to form a prediction and what are the properties of this transformation constitute fundamental questions in the theory of deep learning. A promising avenue to understand the hidden mechanisms of DNNs is Neural Collapse (NC) (Papayan et al., 2020). NC is a widely observed structural property of overparametrized DNNs, occurring in the terminal phase of gradient descent training on classification tasks. This property is linked with the performance of DNNs, such as generalization and robustness (Papayan et al., 2020; Su

et al., 2023). NC is defined by four properties that describe the geometry of feature representations of the training data in the last layer. Of these, in this paper we focus on the following two, because they are relevant in the context of deeper layers. The *within-class variability collapse* (NC1) states that feature vectors of the training samples within a single class collapse to the common class-mean. The *orthogonality or simplex equiangular tight frame property* (NC2) states that these class-means form an orthogonal or simplex equiangular tight frame. While initially observed in just the final hidden layer, these properties were measured for the intermediate layers of DNNs as well (Rangamani et al., 2023; He & Su, 2022), indicating that NC progresses depth-wise. This has led to the definition and study of the Deep Neural Collapse (DNC), a direct depth-wise extension of the standard Neural Collapse (Súkeník et al., 2023).

The theoretical explanations of the formation of (D)NC have mostly relied on a data-agnostic model, known as *unconstrained features model* (UFM) (Mixon et al., 2020; Lu & Steinerberger, 2022). This assumes that DNNs are infinitely expressive and, thus, optimizes for the feature vectors in the last layer directly. The deep UFM (DUFM) was then introduced to account for more layers (Súkeník et al., 2023; Tirer & Bruna, 2022). The (D)UFM has been identified as a useful analogy for neural network collapse, as (D)NC emerges naturally in this setting for a variety of loss functions and training regimes (see Section 2). The (D)NC has been proven to emerge or be optimal under (D)UFM in various settings – under different loss functions, training regimes and in different senses, see Section 2. However, (D)UFM discards the training data and most of the network completely, thus ignoring also the role of feature learning in DNC. This is a serious gap to fully understand the formation of DNC in the context of the full DNN pipeline.

In this paper, we argue that feature learning is responsible for inducing DNC in trained neural networks. To argue this, we first give substantial evidence that within-class variability collapse in DNNs is primarily caused by the application of the right singular vectors of the weight matrix and the subsequent multiplication with its singular values (Section 4). This is in opposition to the belief that neural collapse improves through layers as a consequence of the application of the non-linearity (Tirer & Bruna, 2022). Indeed, if  $W$  is a full rank matrix, then the common metric of within-class

---

<sup>\*</sup>Equal contribution <sup>1</sup>Department of Computer Science, University of California San Diego, San Diego, USA <sup>2</sup>Institute of Science and Technology Austria, Klosterneuburg, Austria. Correspondence to: Daniel Beaglehole <dbeaglehole@ucsd.edu>, Peter Súkeník <peter.sukenik@ista.ac.at>.

variability for  $X$  (the neural representations that are multiplied by  $W$ ) and  $WX$  are equal. Thus, the only way in which the application of a linear layer reduces the within-class variability is by erasing the within-class differences via the small singular directions of  $W$ . This operation can be viewed as discarding irrelevant information, or denoising, a form of feature learning.

The small singular directions of  $W$  are defined by its right singular vectors and singular values. Therefore, it is fully deducible from the Gram matrix of the weights at each layer,  $W^\top W$ . Radhakrishnan et al. (2022); Beaglehole et al. (2023) have identified that, in many settings and across all layers of the network,  $W^\top W$  is approximately proportional to the average gradient outer product (AGOP) with respect to the inputs to that layer, in a statement termed the *Neural Feature Ansatz* (NFA). The NFA suggests that neural networks extract features from the data representations at every layer by projection onto the AGOP with respect to that layer.

Recent work then incorporated layerwise linear transformation with the AGOP into kernel machines, such as the neural tangent kernel (Jacot et al., 2018), to model the deep feature learning mechanism of neural networks (Beaglehole et al., 2023). The output of their backpropagation-free method, Deep Recursive Feature Machines (Deep RFM), is a standard, randomly initialized neural network, where each random weight matrix is additionally right-multiplied by the AGOP of a kernel machine. Their method was shown to improve performance of convolutional kernels on vision datasets and recreate the edge detection ability of convolutional neural networks.

Strikingly, we show that the neural network generated by this very same method, Deep RFM, exhibits deep neural collapse (Section 5). We link the mechanism of DNC formation between DNNs and Deep RFM by demonstrating that projection onto the AGOP is responsible for most of the DNC metric improvement in Deep RFM both empirically and theoretically. Our results demonstrate that (i) AGOP is the mechanism of DNC in Deep RFM, and (ii) when the NFA holds, the right singular structure of  $W$ , and therefore the AGOP, induces within-class variability collapse in DNNs. We thus establish feature learning through the AGOP as a plausible mechanism for DNC in DNNs.

We verify these claims with an extensive experimental evaluation, which demonstrates a consistent formation of DNC in Deep RFMs across several vision datasets. Additionally, we provide a theoretical analysis that explains this mechanism in the asymptotic high-dimensional regime and the smaller data regime under additional assumptions. The first analysis is based on the approximate linearity of kernel matrices in the regime of large number of data samples and dimension. We argue in our second analysis that the formation of DNC

in Deep RFMs is optimal in the kernel ridge regression sense. Further, if the data is already partially grouped into clusters (as assumed in (Seleznova et al., 2023)), we show how the AGOP can strengthen the DNC from one layer to the next.

## 2. Related work

**Neural collapse (NC).** Since the seminal paper by Papayan et al. (2020), the phenomenon of neural collapse has attracted significant attention. Hui et al. (2022) argue that NC does not generalize to the test set. Galanti et al. (2022) use NC to improve generalization bounds for transfer learning, while Wang et al. (2023) discuss transferability capabilities of pre-trained models based on their NC on the target distribution. Haas et al. (2022) argue that NC can lead to improved OOD detection. Connections between robustness and NC are discussed in (Su et al., 2023). For a survey, we refer the interested reader to (Kothapalli, 2023).

The main theoretical framework to study the NC is the Unconstrained Features Model (UFM) (Mixon et al., 2020; Lu & Steinerberger, 2022). Under this framework, many works have shown the emergence of the NC, either via optimality and/or loss landscape analysis (Weinan & Wojtowysch, 2022; Lu & Steinerberger, 2022; Zhou et al., 2022), or via the study of gradient-based optimization (Ji et al., 2022; Han et al., 2022; Wang et al., 2022). Some papers also focus on the generalized class-imbalanced setting, where the NC does not emerge in its original formulation (Thrapoulidis et al., 2022; Fang et al., 2021; Hong & Ling, 2023). Deviating from the strong assumptions of the UFM model, a line of work focuses on gradient descent in homogeneous networks (Poggio & Liao, 2020; Xu et al., 2023; Kunin et al., 2022), while others introduce perturbations (Tirer et al., 2022).

Crucially, it was soon noticed that NC propagates to earlier layers of DNNs, as opposed to just being a phenomenon of the last layer. He & Su (2022); Rangamani et al. (2023); Parker et al. (2023) show the presence of the DNC in DNNs in various training regimes. Theoretical works have then tried to extend the theory to reach beyond the last layer. A deep linear UFM is considered by (Dang et al., 2023) and the optimality of DNC is proved under various regimes. The first work to study deep non-linear ReLU-activated UFM is by Sůkeník et al. (2023), where the authors show the optimality of DNC across the whole depth for the deep UFM in binary classification.

**AGOP feature learning.** The NFA was shown to capture many aspects of feature learning in neural networks including improved performance and interesting structural properties. The initial work on the NFA connects it to the emergence of spurious features and simplicity bias, why pruning DNNs may increase performance, the “lottery ticket

hypothesis”, and a mechanism for grokking in vision settings (Radhakrishnan et al., 2022). Zhu et al. (2023) connect large learning rates and catapults in neural network training to better alignment of the AGOP with the true features. Radhakrishnan et al. (2024) demonstrate that the AGOP recovers the implicit bias of deep linear networks toward low-rank solutions in matrix completion. Beaglehole et al. (2024) identify that the NFA is due to alignment of the weights to the pre-activation tangent kernel and introduce an intervention to improve NFA feature learning.

### 3. Preliminaries

#### 3.1. Notation

For simplicity, we assume a class-balanced setting, where  $N = Kn$  is the total number of training samples, with  $K$  being the number of classes and  $n$  the number of samples per class. Let us order the training samples such that the labels  $Y \in \mathbb{R}^{K \times N}$  can be written as  $I_K \otimes \mathbf{1}_n^\top$ , where  $I_K$  denotes a  $K \times K$  identity matrix,  $\otimes$  denotes the Kronecker product and  $\mathbf{1}_n$  a row vector of all-ones of length  $n$ . For a matrix  $A$  and a column vector  $v$ , the operation  $A \oplus v$ , divides each row of  $A$  by the corresponding element of  $v$ .

Both a DNN and Deep RFM of depth  $L$  can be written as:

$$f(x) = W_{L+1} \sigma(m_L \sigma(m_{L-1} \dots \sigma(m_1(x)) \dots)),$$

where  $m_l$  is a matrix and  $\sigma$  is the ReLU activation function. If the matrix  $m_l$  is defined by a single matrix, as in fully-connected networks, and not a product, we denote it by a weight matrix  $W_l$ . Each weight matrix is decomposed via its SVD as  $W_l = U_l S_l V_l^\top$ . The training data  $X_1 \in \mathbb{R}^{d_1 \times N}$  is stacked into columns and we let  $X_l, \tilde{X}_l, l \geq 2$  be the feature representations of the training data after  $l$  layers of the DNN after and before the non-linearity, respectively.

#### 3.2. Deep Neural Collapse

We define the feature vectors  $x_{ci}^l$  of the  $i$ -th sample of the  $c$ -th class as the input to  $m_l$ . Then,  $\tilde{x}_{ci}^l$  are the feature vectors produced from  $m_{l-1}$  before the application of  $\sigma$ , and are defined only for  $l > 1$ . Let  $\mu_c^l := \frac{1}{n} \sum_{i=1}^n x_{ci}^l$ ,  $\tilde{\mu}_c^l := \frac{1}{n} \sum_{i=1}^n \tilde{x}_{ci}^l$  be the corresponding class means, and  $H_l, \tilde{H}_l \in \mathbb{R}^{d_l \times K}$  the matrices of class means. We will also consider the centered and normalized class means  $\bar{H}_l = (H_l - \mu_G^l) \oplus (H_l - \mu_G^l)$ , where  $\mu_G^l$  is the global feature mean at layer  $l$ . NC1 is defined in terms of two metrics:

$$\begin{aligned} \Sigma_W^l &= \frac{1}{N} \sum_{c=1}^K \sum_{i=1}^n (x_{ci}^l - \mu_c^l)(x_{ci}^l - \mu_c^l)^\top, \\ \Sigma_B^l &= \frac{1}{K} \sum_{c=1}^K (\mu_c^l - \mu_G^l)(\mu_c^l - \mu_G^l)^\top, \end{aligned}$$

i.e., the *within-class* and *between-class* variability at layer  $l$ .

**Definition 3.1.** In the context of this work, the neural collapse at layer  $l$  is achieved if the following two properties are satisfied:

- **DNC1:** The within-class variability at layer  $l$  is 0. This property can be stated for the features either after or before the application of the activation function  $\sigma$ . In the former case, the condition requires  $x_{ci}^l = x_{cj}^l$  for all  $i, j \in \{1, \dots, n\} \triangleq [n]$  (or, in matrix notation,  $X_l = H_l \otimes \mathbf{1}_n^\top$ ); in the latter,  $\tilde{x}_{ci}^l = \tilde{x}_{cj}^l$  for all  $i, j \in [n]$  (or, in matrix notation,  $\tilde{X}_l = \tilde{H}_l \otimes \mathbf{1}_n^\top$ ).
- **DNC2:** The class-means at the  $l$ -th layer form either an orthogonal basis or a simplex equiangular tight frame (ETF). As for DNC1, this property can be stated for features after or before  $\sigma$ . We write the ETF class-mean covariance  $\Sigma_{\text{ETF}} \triangleq (1 + \frac{1}{K-1})I_K - \frac{1}{K-1}\mathbf{1}_K\mathbf{1}_K^\top$ . In the former case, the condition requires either  $H_l^\top H_l \propto I_K$  or  $H_l^\top H_l \propto \Sigma_{\text{ETF}}$ ; in the latter  $\tilde{H}_l^\top \tilde{H}_l \propto I_K$  or  $\tilde{H}_l^\top \tilde{H}_l \propto \Sigma_{\text{ETF}}$ .

#### 3.3. Average gradient outer product

The AGOP is a statistic defined with respect to a dataset  $X \in \mathbb{R}^{d_o \times N}$  and any model, that accepts inputs from the data domain  $f : \mathbb{R}^{d_o \times 1} \rightarrow \mathbb{R}^{K \times 1}$ , where  $K$  is the number of outputs. By writing the Jacobian of the model outputs with respect to its inputs at layer  $l$  as  $\frac{\partial f(x)}{\partial x^l} \in \mathbb{R}^{d_o \times K}$ , we define the AGOP as an operator on  $f$  and  $X$ :

$$\text{AGOP}(f, X) \triangleq \frac{1}{N} \sum_{c=1}^K \sum_{i=1}^N \frac{\partial f(x_{ci})}{\partial x} \frac{\partial f(x_{ci})^\top}{\partial x}.$$

This object has important implications for learning, in part, because the AGOP of a predictor that has somewhat learned the target function will resemble the *expected* gradient outer product (EGOP) of the target function (Yuan et al., 2023). While the AGOP is specific to a model and training data, the EGOP is an operator on the population distribution and the function to be estimated. The EGOP contains specific useful information about the target and data distribution, such as low-rank structure, that improves prediction.

Remarkably, it was identified in (Radhakrishnan et al., 2022; Beaglehole et al., 2023) that neural networks will automatically estimate the AGOP in the Gram matrix of the weights in all layers of the neural network. Stated formally, the authors observe the Neural Feature Ansatz, here posed for fully-connected architectures.

**Ansatz 3.2** (Neural Feature Ansatz (Radhakrishnan et al., 2022)). *Let  $f$  be a depth- $L$  neural network trained on data*

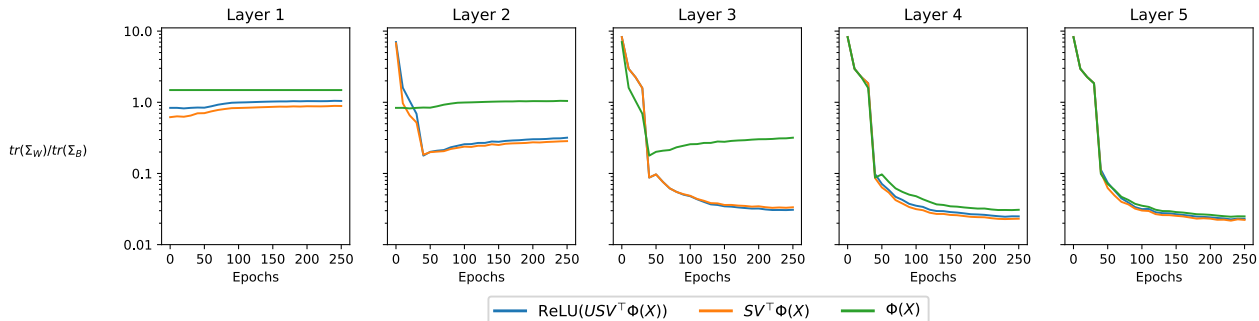


Figure 1. Feature variability collapse from different singular value decomposition components on CIFAR-10. We measure the reduction in the NC1 metric throughout training at each layer of an MLP with  $L = 5$ . Each layer is decomposed into its input,  $\Phi(X)$ , projection onto the right singular space of  $W$ ,  $SV^T\Phi(X)$ , and then  $U$ , the left singular vectors of  $W$ , and application of ReLU.

$X$  using stochastic gradient descent. Then, for all layers  $l \in [L]$ ,

$$W_l^T W_l \propto \frac{1}{N} \sum_{c=1}^K \sum_{i=1}^n \frac{\partial f(x_{ci})}{\partial x^l} \frac{\partial f(x_{ci})}{\partial x^l}^T.$$

Crucially, the AGOP can be defined for any differentiable estimator, not necessarily a neural network. For example, prior work considers the AGOP of general non-parametric methods (Trivedi et al., 2014). In (Radhakrishnan et al., 2022), the authors introduce a kernel learning algorithm, the Recursive Feature Machine (RFM), that performs kernel regression and estimates the AGOP in an alternating fashion, modeling the NFA feature learning mechanism of fully-connected networks.

Subsequent work introduced the Deep Recursive Feature Machine (Deep RFM) to model deep feature learning in neural networks (Beaglehole et al., 2023). Deep RFM recursively generates representations by transforming the input to that layer with the AGOP of the model w.r.t. this input, itself estimated from shallow RFM, and then applying a random feature map. To define the Deep RFM, let  $\{k_l\}_{l=1}^{L+1} : \mathbb{R}^{d_l \times d_l} \rightarrow \mathbb{R}$  be a set of kernels. For the ease of notation, we will write  $k_l(X_l, X_l)$  for a matrix of kernel evaluations between columns of  $X_l$ . Then, the Deep RFM is described in Algorithm 1.

Note that the Deep RFM as defined here is less general than the version in (Beaglehole et al., 2023), as we are considering only one AGOP estimation step in the inner-optimization of RFM. The high-dimensional feature maps  $\Phi_l(\cdot)$  are usually realized as  $\sigma(W_l \cdot)$ , where  $W_l$  is a matrix with standard Gaussian entries, thus  $\Phi_l$  serves as a random features generator.

The single loop in the Deep RFM represents a reduced RFM learning process. The RFM itself is based on kernel ridge regression, therefore we introduce the ridge coefficient  $\mu$ . The training procedure of RFM is meant to perform well

---

#### Algorithm 1 Deep Recursive Feature Machine (Deep RFM)

---

**input**  $X_1, Y, \{k_l\}_{l=1}^{L+1}, L, \{\Phi_l\}_{l=1}^L$  {kernels:  $\{k_l\}_l$ , depth:  $L$ , feature maps:  $\{\Phi_l\}_l$ }  
**output**  $\alpha_{L+1}, \{M_l\}_{l=1}^L$   
**for**  $l \in 1, \dots, L$  **do**  
     Normalize the data,  $X_l \leftarrow X_l \ominus \|X_l\|$   
     Learn coefficients,  $\alpha_l = Y(k_l(X_l, X_l) + \mu I)^{-1}$ .  
     Construct predictor,  $f_l(\cdot) = \alpha_l k_l(\cdot, X_l)$ .  
     Compute AGOP:  $M_l = \sum_{c,i=1}^{K,n} \nabla f_l(x_{ci}^l) \nabla f_l(x_{ci}^l)^T$ .  
     Transform the data  $X_{l+1} \leftarrow \Phi_l(M_l^{1/2} X_l)$ .  
**end for**  
 Normalize the data,  $X_{L+1} \leftarrow X_{L+1} \ominus \|X_{L+1}\|$   
 Learn coefficients,  
 $\alpha_{L+1} = Y(k_{L+1}(X_{L+1}, X_{L+1}) + \mu I)^{-1}$ .

---

in the corresponding kernel ridge regression which will be particularly important in Section 5.4.

## 4. Deep Neural Collapse as an effect of linear denoising

There are precisely two ways that DNNs can discard unnecessary information in the data, such as noise or spurious features. One of them is through non-linearities, i.e., ReLU, where negative entries are erased. The other one is through the small eigendirections of  $W_l^T W_l$  or, approximately, the non-trivial null space of  $W_l$ , where components of vectors that belong to the null space are discarded. If we write again the SVD  $W_l = U_l S_l V_l^T$ , then  $S_l V_l^T$  is the part with possibly non-trivial null space. This right singular component can be viewed as the *feature extraction* part of the linear layer. In contrast, the multiplication with  $U_l$  simply rotates or reflects the prior representation.

All parts of the process, together with the ReLU, are important for neural network predictions. However, the DNC1 can only improve through the  $S_l V_l^T$  multiplication and the

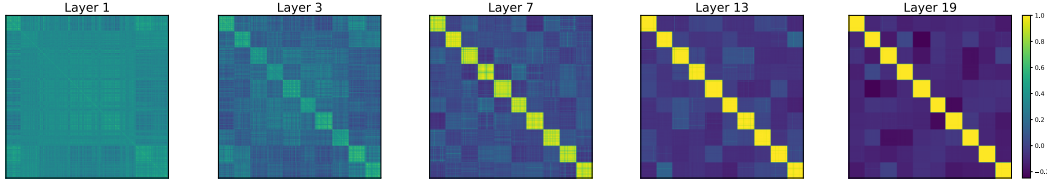


Figure 2. Neural collapse with Deep RFM on 2000 points from CIFAR-10. The  $2000 \times 2000$  matrix of inner products of all pairs of points in  $X_l$  extracted from layers  $l \in \{1, \dots, 19\}$  of Deep RFM following centering by the global mean  $\mu_G^l$  and normalizing each point to the unit sphere. The data are ordered in blocks so that points of the same class are adjacent to one another, arranged from class 1 to class 10. All points of the same class have inner products approximately equal to 1 at the final layer  $l = 19$  (are equal to each other), while points of different classes have inner products approximately  $-\frac{1}{K-1}$ , for each of the  $K = 10$  classes.

ReLU application. In particular, considering the standard DNC1 metric  $\text{tr}(\Sigma_W)/\text{tr}(\Sigma_B)$  (Rangamani et al., 2023), a simple computation gives

$$\frac{\text{tr}(\hat{\Sigma}_W)}{\text{tr}(\hat{\Sigma}_B)} = \frac{\text{tr}(U\Sigma_W U^\top)}{\text{tr}(U\Sigma_B U^\top)} = \frac{\text{tr}(\Sigma_W)}{\text{tr}(\Sigma_B)}.$$

Here, the  $\Sigma$  matrices refer to the within-class variability after the application of  $SV^\top$ , while the  $\hat{\Sigma}$  matrices correspond to the output of the full linear layer. The first equality holds due to the linearity and the second due to the cyclic property of the trace.

While both ReLU and  $S_l V_l^\top$  can influence the DNC1 metric, our experiments show that  $S_l V_l^\top$  induces the majority of within-class variability collapse. We verify this claim by plotting the DNC1 metrics of all layers of a fully-connected network trained on CIFAR-10 (Figure 1, see Appendix B for similar results on MNIST and SVHN), where each layer is decomposed into its different parts – (1) the input to that layer, (2) the embedding after multiplication with  $S_l V_l^\top$ , and (3) the embedding after multiplication with the left singular vectors and application of the ReLU. We see here the the ratio of within-class to between-class variability decreases mostly between steps (1) and (2), on application of the right singular structure. This has profound implications for both neural collapse and feature learning. It shows that, counter-intuitively, DNNs cancel most of the intra-class sample differences (which, assuming neural collapse preserves task-relevant information, is the irrelevant variation in the data) by the linear weight matrix, and not the non-linear ReLU.

Since these results are in a regime where the NFA holds with high correlation (see Appendix B), we know that  $S_l V_l^\top$  will project into a very similar space as the AGOP. Therefore, AGOP performs linear denoising that significantly decreases the within-class variability, further supporting its importance in feature learning.

Unlike DNC1, we have observed a strong DNC2 progression only in the very last layer. This is due to the fact that DNC2 was observed in the related work (Rangamani et al., 2023; Parker et al., 2023) in a regime of large initialization.

In contrast, the NFA holds in a regime of small initialization (Radhakrishnan et al., 2022; Beaglehole et al., 2023), and in this small initialization (or feature learning) regime, the low-rank bias prevents strong collapse from occurring, see Li et al. (2020) for a good intuition on the low-rank bias.

## 5. Deep Neural Collapse in Deep Recursive Feature Machines

We have given evidence that the improvement in neural collapse for DNNs is induced by the AGOP. We now demonstrate that AGOP is a mechanism for DNC in the Deep RFM model, which was proposed in prior work as an abstraction for deep feature learning in DNNs via the layerwise introduction of AGOP. We first demonstrate empirically that Deep RFM exhibits DNC - NC1 and NC2 - and that the induction of DNC is due to the application of AGOP. We additionally formally establish that the reduction in within-class variability cannot be due to the application of the random feature map. Finally, we prove theoretically in an asymptotic and non-asymptotic setting that DNC will occur as a consequence of Deep RFM.

### 5.1. Empirical evidence

We first visualize the formation of DNC in the input vectors of across each layer of Deep RFM. In Figure 2, we show the Gram matrix,  $\bar{X}_l \bar{X}_l^\top$ , of centered and normalized feature vectors  $\bar{X}_l = (X_l - \mu_G^l) \oplus \|X_l - \mu_G^l\|$  extracted from several layers of Deep RFM, exactly as presented in Algorithm 1 and trained on 2000 points from CIFAR-10. After 18 layers of DeepRFM, the final Gram matrix is approximately equal to that of perfectly collapsed data - all points are at exactly their class means, and the class means form an ETF.

We then apply Deep RFM to full CIFAR-10, and show collapse occurring as a consequence of projection onto the square root of the AGOP,  $M_l^{1/2}$  (Figure 3). We observe that the improvement in NC1 is entirely due to  $M_l^{1/2}$ , and

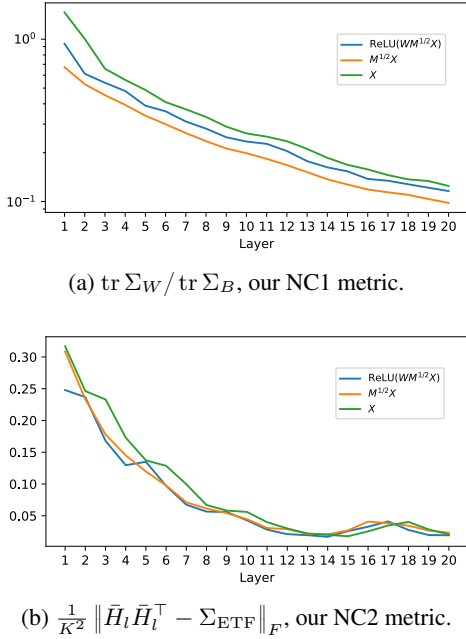


Figure 3. Neural collapse with Deep RFM on full CIFAR-10 across 20 layers. We plot the NC1 and NC2 metrics across feature vectors  $X_l$ ,  $M_l^{1/2}X_l$ , and  $\sigma(W_l M_l^{1/2}X_l)$ . Plot (a) is on a log scale, while plot (b) is with a linear scale.

the random feature map actually worsens the NC1 value. Similarly, the majority of improvement in NC2, measured by  $\frac{1}{K^2} \|\bar{H}_l \bar{H}_l^\top - \Sigma_{\text{ETF}}\|_F$ , is due to multiplication with this matrix. These results are consistent with the crucial point that Deep RFM deviates from a simple deep random feature model by additionally projecting onto the AGOP, and we do not expect a random feature model to induce neural collapse (as we will derive in Section 5.2). Note that these observations are consistent across datasets (see Appendix B).

## 5.2. Random features cannot significantly reduce within-class variability

In the following proposition, we prove that the random features mapping with ReLU influences the within- and between-class variabilities only marginally and if anything, it makes the DNC1 metrics slightly worse.

**Proposition 5.1.** *Let  $x, y \in \mathbb{R}^d$  be two fixed vectors of unit length. Let  $W \in \mathbb{R}^{D \times d}$  be a weight matrix whose entries are initialized i.i.d. from  $\mathcal{N}(0, 2/D)$ . Assume  $x^\top y = r$ . Then,*

$$\mathbb{E}(\sigma(Wx)^\top \sigma(Wy)) = \frac{(1-r^2)^{3/2}}{\pi} + \frac{r^2 \sqrt{1-r^2}}{\pi} + \frac{r}{2} + \frac{r}{\pi} \arctan\left(\frac{r}{\sqrt{1-r^2}}\right). \quad (1)$$

Moreover, the variance of this dot product scales with

$1/D$ , and the product is sub-exponential, making it well-concentrated.

The proof is a direct computation, which is deferred to Appendix A.

This proposition gives a relationship between the dot product  $x^\top y$  of two vectors and the dot product of the outputs of their corresponding random feature maps  $\sigma(Wx)^\top \sigma(Wy)$ . This is relevant because for unit vectors, the dot product is a direct indication of the distance between the two vectors. In Figure 4 (left), we plot a function which takes the distance between two unit vectors  $x, y$  and outputs the expected distance between their feature maps  $\sigma(Wx), \sigma(Wy)$ . While the distance in the input space ranges between 0 (aligned vectors) and 2 (counter-aligned vectors), in the output space the maximum is  $\sqrt{2}$  due to the ReLU activation. However, importantly, we see that the expected distance between  $\sigma(Wx)$  and  $\sigma(Wy)$  is bigger than the corresponding linear interpolation, and the ratio

$$\frac{\mathbb{E}[\|\sigma(Wx) - \sigma(Wy)\|]}{\|x - y\|},$$

is monotonically decreasing and lies in an interval  $[1/\sqrt{2}, 1]$ , as indicated in the Figure 4 (right), see also (Liu & Hui, 2023) for similar considerations.

This means that the distances between data points generally increase, but not drastically. They increase irrespective of the angle between data points, however they tend to expand relatively more, if the data points are already aligned. Therefore, the DNC1 metric should on average marginally increase or stay constant. This is in agreement with our Deep RFM measurements on all vision datasets (Figure 3 and Appendix B). Importantly, this also supports the connection between neural networks and Deep RFM, since in DNNs the DNC1 metric also doesn't significantly change after applying the ReLU (Figure 1).

The key phenomenon in the DNC formation is thus the feature learning through the AGOP (explicitly in Deep RFM), which is aligned with the right singular space and singular values in DNNs due to the NFA.

## 5.3. Asymptotic analysis

Many works have derived that, under mild conditions on the data and kernel, non-linear kernel matrices of high dimensional data are well approximated by linear kernels with a non-linear perturbation (Karoui, 2010; Adlam et al., 2019; Hu & Lu, 2022). In this section, we provide a proof that Deep RFM will induce DNC when the non-linear kernels  $\{k_l\}_l$  and feature maps  $\{\Phi_l\}_l$  satisfy this property. In particular, in the high-dimensional setting in these works, non-linear kernel matrices written  $k(X) := k(X, X)$  for

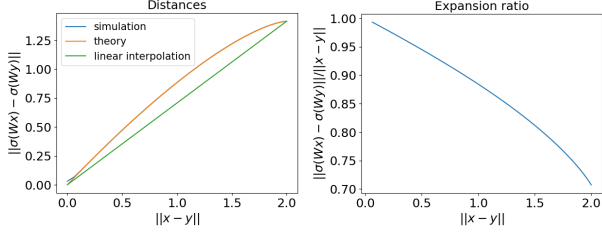


Figure 4. The relationship between  $\|x - y\|$  and  $\mathbb{E}(\|\sigma(Wx) - \sigma(Wy)\|)$ . On the left, we see the direct relationship between these two quantities compared with the linear interpolation (green). The theoretical computation (orange) and the simulation result (blue) match almost perfectly.

simplicity, are well approximated by

$$k(X) \approx \gamma_k \mathbf{1}\mathbf{1}^\top + X^\top X + \lambda_k I,$$

where  $\lambda_k, \gamma_k > 0$ . Following (Adlam & Pennington, 2020), for additional simplicity we consider centered kernels,

$$k_{\text{lin}}(X) \equiv X^\top X + \lambda_k I.$$

We analyze the Deep RFM with two slight modifications: (i) we don’t normalize the data at each iteration, and (ii) we scale the data by a value  $\kappa^{-1}$  at each iteration. The recursive procedure begins with a dataset  $X_l$  at layer  $l$  in Deep RFM, and constructs  $\tilde{X}_l$  from the AGOP  $M_l$  of the kernel ridgeless regression solution,

$$\tilde{X}_{l+1}^\top \tilde{X}_{l+1} = \kappa^{-1} X_l^\top M_l X_l,$$

for  $\kappa = 1 - 2\lambda_k(1 + \lambda_\Phi^{-1})$ . Then, we will apply a non-linear feature map  $\Phi_{\text{lin}}$  corresponding to a kernel  $k_\Phi$  that exhibits a similar linearization on the data. For  $k_\Phi$ , we introduce a new parameter  $\lambda_\Phi$  capturing the deviation of this feature map from linearity, and write the corresponding Gram matrix

$$\begin{aligned} X_{l+1}^\top X_{l+1} &= \Phi_{\text{lin}}(\tilde{X}_{l+1})^\top \Phi_{\text{lin}}(\tilde{X}_{l+1}) \\ &\equiv k_\Phi(\tilde{X}_{l+1}) \\ &= \tilde{X}_{l+1}^\top \tilde{X}_{l+1} + \lambda_\Phi I, \end{aligned}$$

where  $\lambda_k, \lambda_\Phi$  are finite and  $\lambda_\Phi \gg \lambda_k > 0$ .

Intuitively, the ratio  $\lambda_k/\lambda_\Phi$  determines how close to linear  $k_{\text{lin}}$  is when applied to the dataset, and therefore the rate of NC. By Assumption 5.3, the scaled gram matrix

$$\bar{G}_l \equiv \lambda_\Phi^{-1} X_l^\top X_l$$

has minimum eigenvalue at least 1. Meanwhile, the scaled kernel matrix has form,

$$\lambda_\Phi^{-1} (X_l^\top X_l + \lambda_k I) = \bar{G}_l + \lambda_k/\lambda_\Phi \cdot I,$$

If  $\lambda_k/\lambda_\Phi$  were exactly 0, then  $(\bar{G}_l + \lambda_k/\lambda_\Phi \cdot I)^{-1}$  is equal to  $\bar{G}_l^{-1} = \lambda_\Phi (X_l^\top X_l)^{-1}$ , the scaled linear regression solution. In this case, collapse will occur in just one layer of Deep RFM, as the AGOP of a linear function is exactly the outer product of the solution with itself. Otherwise, if this ratio were large, i.e.  $\lambda_k/\lambda_\Phi = \Omega(1)$ ,  $(\bar{G}_l + \lambda_k/\lambda_\Phi \cdot I)^{-1}$  can be far from the linear regression solution. In this case, the kernel regression solution contains non-linear variation that increases the rank of the AGOP (preventing collapse). Between these limits, a larger  $\lambda_k$  delays collapse as a function of the number of layers of Deep RFM, while larger  $\lambda_\Phi$  accelerates collapse. Note that this theory offers an explanation why a non-linear activation is needed for DNC:  $\lambda_\Phi = 0$  with a linear feature map.

We provide a simple interpretation for why non-linear feature maps introduce an identity term  $\lambda_\Phi I$  to the data Gram matrix. As in our experiments on Deep RFM where  $\Phi(x) = \sigma(Wx)$ , the random feature map separates all pairs of data points, especially nearby ones, lowering the off-diagonal entries in the empirical kernel and increasing the effective rank of this matrix (Figure 4).

Having established our simplified Deep RFM, we prove that DNC occurs in the following full-rank, high-dimensional setting.

**Assumption 5.2** (Data is high dimensional). We assume that the data has dimension  $d \geq n$ .

**Assumption 5.3** (Data is full rank). We assume that the initial data Gram matrix  $X_1^\top X_1$  has minimum eigenvalue at least  $\lambda_\phi > 0$ . Otherwise the theorem holds for  $l > 2$ , after the non-linear feature map is applied.

Our analysis requires these assumptions to guarantee  $(X_l^\top X_l)^{-1}$  is stable (i.e. it exists and has maximum eigenvalue  $\lambda_\Phi^{-1}$  at every iteration) for all  $l$ . Our setup can be viewed as a “beyond-worst-case” theoretical analysis (Roughgarden, 2019), where inputs are taken to be arbitrary followed by perturbation with a “smoothing” parameter  $\lambda_\Phi$  (Spielman & Teng, 2004). Our empirical evidence for Deep RFM on real datasets, where  $n > d$ , suggests that these assumptions can be relaxed using a more refined analysis.

We present our main theorem.

**Theorem 5.4** (Deep RFM exhibits neural collapse). *Suppose we apply Deep RFM on any dataset with  $\{\Phi_l\}_l$  and  $\{k_l\}_l$  all chosen as the feature map  $\Phi_{\text{lin}}$  and kernel  $k_{\text{lin}}$  above, with no ridge parameter ( $\mu = 0$ ). Then, there exists a universal constant  $C > 0$ , such that for any  $0 < \epsilon \leq 1$ , provided  $\lambda_k \leq \frac{C\lambda_\Phi}{2(1+\lambda_\Phi^{-1})^n}(1 - \epsilon)$ , and for all layers  $l \in \{2, \dots, L\}$  of Deep RFM,*

$$\|\tilde{X}_{l+1}^\top \tilde{X}_{l+1} - yy^\top\| \leq (1 - \epsilon) \|\tilde{X}_l^\top \tilde{X}_l - yy^\top\| + O(\lambda_k^2 \lambda_\Phi^{-2}).$$

Note that this theorem immediately implies exponential con-

vergence to NC1 and NC2 up to error  $O(L\lambda_k^2\lambda_\Phi^{-2})$ , a small value determined by the parameters of the problem. As a validation of our theory, we see that this exponential improvement in the DNC metric occurs in all layers (Figure 3).

The proof for this theorem is roughly as follows. Recall that, by our argument earlier in this section, a linear kernel will cause collapse within just one layer of Deep RFM. However, in the more general case we consider, a small non-linear deviation from a linear kernel,  $\lambda_k$ , is introduced. Beginning with the first layer, partial collapse occurs if the ratio  $\lambda_k\lambda_\Phi^{-1}$  is sufficiently small. Following the partial collapse, in subsequent layers, the data Gram matrix will sufficiently resemble the collapsed matrix, so that the non-linear kernel solution on the collapsed data will behave like the linear solution, leading to further convergence to the collapsed data Gram matrix, a fixed point of the Deep RFM iteration (Lemma A.2).

#### 5.4. Non-asymptotic analysis

Next, we show that the formation of the neural collapse is not only implicitly given by the specific optimization procedure of the Deep RFM, but is also implicitly regularized for in the parametrized kernel ridge regression, a model class that includes RFM (i.e., a single layer of Deep RFM). Consider a parametrized kernel on  $\mathbb{R} \times \mathbb{R}$  of the form  $k_M(x, y) = \phi(\|x - y\|_M^2)$ , where  $\|x - y\|_M^2 = (x - y)^\top M(x - y)$ ,  $\phi$  is a strictly decreasing, strictly positive univariate function s.t.  $\phi(0) = 1$ , and  $k_M$  is a valid kernel for any symmetric positive semi-definite  $M$ . Let  $\mathcal{H}_M$  be the corresponding reproducing kernel Hilbert space (RKHS). Then, by the parametrized kernel ridge regression, we mean the following optimization problem from Chen et al. (2023) over all possible  $M$  and  $\alpha \in \mathbb{R}^{n \times K}$ :

$$\min_{f, M} \frac{1}{2} \|f(X) - Y\|^2 + \frac{\mu}{2} \|f\|_{\mathcal{H}_M}^2. \quad (2)$$

Using the representer theorem (Schölkopf et al., 2001), the optimal solution of Problem 2 can be written as

$$f^*(z) = \sum_{c, i=1, 1}^{K, n} \alpha_{ci}^* k_{M^*}(x_{ci}, z).$$

We can re-formulate Problem 2 as the following finite-dimensional optimization problem:

$$\min_{\alpha, M} \alpha^\top (k_M^2 + \mu k_M) \alpha - 2\alpha^\top k_M y, \quad (3)$$

where  $k_M := k_M(X, X)$  is the matrix of pair-wise kernel evaluations on the data and  $y$  are labels organized into a column. Since we do not explicitly regularize  $M$ , we will drop the dependence on it, treat  $k$  as a free optimization variable and compute the optimal value of the following

relaxed problem:

$$\min_{\alpha, k} \alpha^\top (k^2 + \mu k) \alpha - 2\alpha^\top k y. \quad (4)$$

We make two final simple assumptions. First, we assume that the kernel  $k$  is positive definite. This assumption is only to allow for simpler mathematical analysis and could be dropped using continuity arguments. Note that even a low-rank  $M$  does not naturally produce singular  $k$ , since  $k$  always has 1's on the diagonal. Second, we assume that the task is binary classification with one-dimensional labels equal to  $\pm 1$ . This assumption is only didactic and can be dropped. Now, we are ready to state the optimality result.

**Theorem 5.5.** *The optimal limiting solution of the Problem 4 is  $k^* = I_2 \otimes (\mathbf{1}_n \mathbf{1}_n^\top) = \frac{1}{2}(yy^\top + \mathbf{1}_{2n} \mathbf{1}_{2n}^\top)$ . Any positive definite  $k$  sufficiently close to this (positive semi-definite) solution is therefore nearly optimal.*

*Proof.* We provide a sketch here and defer the detailed proof to Appendix A. Assuming positive definiteness of  $k$ , the conditionally optimal  $\alpha^*|k$  is explicitly computable. Plugging back into the objective and simplifying, we get:

$$\max_k y^\top (k + \mu I)^{-1} k y.$$

Let  $VSV^\top$  be the eigenvalue decomposition of  $k$ . Then, we can equivalently rewrite this objective to:

$$\sum_{i=1}^{2n} (y^\top v_i)^2 \frac{\lambda_i}{\lambda_i + \mu}. \quad (5)$$

By continuity of the Problem 4 in both variables, we can without loss of generality plug  $k^*$  into this, despite it being low-rank (for details see Appendix A). The function value in this case would equal  $2n \frac{n}{n+\mu}$ . We show that any symmetric p.s.d. kernel  $k$  cannot achieve better objective value.

Note that  $\sum_{i=1}^{2n} (y^\top v_i)^2 = 2n$ , since  $(v_i)_{i=1}^{2n}$  forms an orthogonal basis and, therefore, a tight frame with constant 1. Moreover,  $\sum_{i=1}^{2n} \lambda_i = 2n$ , since the diagonal entries of  $k$  are by definition all equal to 1. After normalizing  $y$  to unit norm, it can be shown that we have a weighted average of  $\lambda_i/(\lambda_i + \mu)$ , where the weights correspond to the alignment between  $y$  and the corresponding eigenvector  $v_i$ . We want  $y$  to be most aligned with the eigenvectors corresponding to the biggest eigenvalues. Note that this is the case for  $k^*$ , where  $y^\top v_i = 0$  for all  $i \geq 3$ , thus all eigenvectors of zero eigenvalue and  $(y^\top v_i)^2 = n$  for the leading two eigenvalues that are both equal  $n$ .

Increasing the value of (5) with a different kernel matrix  $k$  would require having at least one of its eigenvalues be bigger than  $n$  (the leading one) and the corresponding alignment  $(y^\top v_1)^2 \geq n$  (see Appendix A). However, this is impossible due to the Perron-Frobenius theorem, which states that a

positive matrix has a simple leading eigenvalue with strictly positive eigenvector (see Appendix A for computations).  $\square$

This result itself, though very general, requires further reasoning to explain the DNC formation through Deep RFM. First, it is not hard to see that there exist matrices  $M$  that cause  $k_M$  to resemble  $k^*$ , if the data is already sufficiently clustered (e.g. after a few layers of Deep RFM or a pre-trained embedding). For example, if  $\|x_{c,i} - x_{c,j}\|^2 \leq A^2, \forall c \in [K]; i, j \in [n]$  and  $\|x_{c,i} - x_{c',j}\|^2 \geq R^3 A^2, \forall c \neq c' \in [K]; i, j \in [n]$ , with  $A > 0, R > 1$ , then just taking  $M = \frac{1}{AR}I$  yields data for which the distances within cluster do not exceed  $R^{-2}$  while distances between clusters exceed  $R$ . Then,  $k_M(x_{c,i}, x_{c,j}) \geq \exp(-R^{-2}) \simeq 1 - R^{-2}$  and  $k_M(x_{c,i}, x_{c',j}) \leq \exp(-R)$ . For sufficiently large  $R$  this would yield the ratio of between- and within-class square distances rising from at least  $R^3$  to at least  $R^4$ .

Second, we argue that RFM naturally minimizes both Problem 3 and Problem 4. This claim is natural since the RFM is a parametrized kernel regression model, where  $M$  is set to be the AGOP, which should minimize (3) as AGOP captures task-specific low-rank structure (Chen et al., 2023). Then, given any setting of  $M$ , RFM is conditionally optimal w.r.t. the parameter  $\alpha$ , as this method simply solves the original kernel regression problem for each fixed  $M$ . Further, we note that choosing  $k$  to be a dot product kernel and  $M$  to be the AGOP of an interpolating linear classifier implies that  $k_M = k^*$ , the optimal solution outlined in Theorem 5.5, by a similar argument to the proof of Theorem 5.4.

## 6. Conclusion

This work is the first to explain the apparent yet never properly understood connection between feature learning and (deep) neural collapse. First, we experimentally show that the DNC1 metric progression through the layers is mostly due to the linear denoising via the application of the center-right singular structure, as opposed to the application of the ReLU as suggested by the feature learning free UFM (Tirer & Bruna, 2022). Under the neural feature ansatz, this highlights the importance of AGOP in the formation of the DNC.

We demonstrate the importance of AGOP in DNC by demonstrating this object induces neural collapse in randomly initialized neural networks through Deep RFM. We validate that AGOP induces NC in Deep RFM both empirically and via asymptotic and non-asymptotic theoretical analyses. The connection is theoretically reinforced by showing that AGOP (as opposed to the random features) is indeed the only part of the Deep RFMs that can cause collapse. Our findings bridge the unsatisfactory gap between the collapse

and the data – with previous work mostly only focusing on the very end of the network and ignoring the training data and its structures.

## Acknowledgements

We acknowledge support from the National Science Foundation (NSF) and the Simons Foundation for the Collaboration on the Theoretical Foundations of Deep Learning through awards DMS-2031883 and #814639 as well as the TILOS institute (NSF CCF-2112665). This work used the programs (1) XSEDE (Extreme science and engineering discovery environment) which is supported by NSF grant numbers ACI-1548562, and (2) ACCESS (Advanced cyberinfrastructure coordination ecosystem: services & support) which is supported by NSF grants numbers #2138259, #2138286, #2138307, #2137603, and #2138296. Specifically, we used the resources from SDSC Expanse GPU compute nodes, and NCSA Delta system, via allocations TG-CIS220009. Marco Mondelli is supported by the 2019 Lopez-Loreta prize.

## References

- Adlam, B. and Pennington, J. The neural tangent kernel in high dimensions: Triple descent and a multi-scale theory of generalization. In *International Conference on Machine Learning*, pp. 74–84. PMLR, 2020.
- Adlam, B., Levinson, J., and Pennington, J. A random matrix perspective on mixtures of nonlinearities for deep learning. *arXiv preprint arXiv:1912.00827*, 2019.
- Beaglehole, D., Radhakrishnan, A., Pandit, P., and Belkin, M. Mechanism of feature learning in convolutional neural networks. *arXiv preprint arXiv:2309.00570*, 2023.
- Beaglehole, D., Mitliagkas, I., and Agarwala, A. Gradient descent induces alignment between weights and the empirical ntk for deep non-linear networks. *arXiv preprint arXiv:2402.05271*, 2024.
- Chen, Y., Li, Y., Liu, K., and Ruan, F. Kernel learning in ridge regression” automatically” yields exact low rank solution. *arXiv preprint arXiv:2310.11736*, 2023.
- Dang, H., Nguyen, T., Tran, T., Tran, H., and Ho, N. Neural collapse in deep linear network: From balanced to imbalanced data. *arXiv preprint arXiv:2301.00437*, 2023.
- Fang, C., He, H., Long, Q., and Su, W. J. Exploring deep neural networks via layer-peeled model: Minority collapse in imbalanced training. In *Proceedings of the National Academy of Sciences (PNAS)*, volume 118, 2021.
- Galanti, T., György, A., and Hutter, M. Improved generalization bounds for transfer learning via neural collapse.

- In *First Workshop on Pre-training: Perspectives, Pitfalls, and Paths Forward at ICML*, 2022.
- Haas, J., Yolland, W., and Rabus, B. T. Linking neural collapse and l2 normalization with improved out-of-distribution detection in deep neural networks. *Transactions on Machine Learning Research (TMLR)*, 2022.
- Han, X. Y., Pappayan, V., and Donoho, D. L. Neural collapse under mse loss: Proximity to and dynamics on the central path. In *International Conference on Learning Representations (ICLR)*, 2022.
- He, H. and Su, W. J. A law of data separation in deep learning. *arXiv preprint arXiv:2210.17020*, 2022.
- Hong, W. and Ling, S. Neural collapse for unconstrained feature model under cross-entropy loss with imbalanced data. *arXiv preprint arXiv:2309.09725*, 2023.
- Hu, H. and Lu, Y. M. Universality laws for high-dimensional learning with random features. *IEEE Transactions on Information Theory*, 69(3):1932–1964, 2022.
- Hui, L., Belkin, M., and Nakkiran, P. Limitations of neural collapse for understanding generalization in deep learning. *arXiv preprint arXiv:2202.08384*, 2022.
- Jacot, A., Gabriel, F., and Hongler, C. Neural tangent kernel: Convergence and generalization in neural networks. In *Conference on Neural Information Processing Systems (NeurIPS)*, 2018.
- Ji, W., Lu, Y., Zhang, Y., Deng, Z., and Su, W. J. An unconstrained layer-peeled perspective on neural collapse. In *International Conference on Learning Representations (ICLR)*, 2022.
- Karoui, N. E. The spectrum of kernel random matrices. *The Annals of Statistics*, pp. 1–50, 2010.
- Kothapalli, V. Neural collapse: A review on modelling principles and generalization. In *Transactions on Machine Learning Research (TMLR)*, 2023.
- Kunin, D., Yamamura, A., Ma, C., and Ganguli, S. The asymmetric maximum margin bias of quasi-homogeneous neural networks. *arXiv preprint arXiv:2210.03820*, 2022.
- Li, Z., Luo, Y., and Lyu, K. Towards resolving the implicit bias of gradient descent for matrix factorization: Greedy low-rank learning. *arXiv preprint arXiv:2012.09839*, 2020.
- Liu, C. and Hui, L. Relu soothes the ntk condition number and accelerates optimization for wide neural networks. *arXiv preprint arXiv:2305.08813*, 2023.
- Lu, J. and Steinerberger, S. Neural collapse under cross-entropy loss. In *Applied and Computational Harmonic Analysis*, volume 59, 2022.
- Mixon, D. G., Parshall, H., and Pi, J. Neural collapse with unconstrained features. *arXiv preprint arXiv:2011.11619*, 2020.
- Pappayan, V., Han, X. Y., and Donoho, D. L. Prevalence of neural collapse during the terminal phase of deep learning training. In *Proceedings of the National Academy of Sciences (PNAS)*, volume 117, 2020.
- Parker, L., Onal, E., Stengel, A., and Intrater, J. Neural collapse in the intermediate hidden layers of classification neural networks. *arXiv preprint arXiv:2308.02760*, 2023.
- Poggio, T. and Liao, Q. Explicit regularization and implicit bias in deep network classifiers trained with the square loss. *arXiv preprint arXiv:2101.00072*, 2020.
- Radhakrishnan, A., Beaglehole, D., Pandit, P., and Belkin, M. Feature learning in neural networks and kernel machines that recursively learn features. *arXiv preprint arXiv:2212.13881*, 2022.
- Radhakrishnan, A., Belkin, M., and Drusvyatskiy, D. Linear recursive feature machines provably recover low-rank matrices. *arXiv preprint arXiv:2401.04553*, 2024.
- Rangamani, A., Lindegaard, M., Galanti, T., and Poggio, T. Feature learning in deep classifiers through intermediate neural collapse. *Technical Report*, 2023.
- Roughgarden, T. Beyond worst-case analysis. *Communications of the ACM*, 62(3):88–96, 2019.
- Schölkopf, B., Herbrich, R., and Smola, A. J. A generalized representer theorem. In *International conference on computational learning theory*, pp. 416–426. Springer, 2001.
- Seleznova, M., Weitzner, D., Giryes, R., Kutyniok, G., and Chou, H.-H. Neural (tangent kernel) collapse. *arXiv preprint arXiv:2305.16427*, 2023.
- Spielman, D. A. and Teng, S.-H. Smoothed analysis of algorithms: Why the simplex algorithm usually takes polynomial time. *Journal of the ACM (JACM)*, 51(3): 385–463, 2004.
- Su, J., Zhang, Y. S., Tsilivis, N., and Kempe, J. On the robustness of neural collapse and the neural collapse of robustness. *arXiv preprint arXiv:2311.07444*, 2023.
- Súkeník, P., Mondelli, M., and Lampert, C. Deep neural collapse is provably optimal for the deep unconstrained features model. *arXiv preprint arXiv:2305.13165*, 2023.

- Thrampoulidis, C., Kini, G. R., Vakilian, V., and Behnia, T. Imbalance trouble: Revisiting neural-collapse geometry. In *Conference on Neural Information Processing Systems (NeurIPS)*, 2022.
- Tirer, T. and Bruna, J. Extended unconstrained features model for exploring deep neural collapse. In *International Conference on Machine Learning (ICML)*, 2022.
- Tirer, T., Huang, H., and Niles-Weed, J. Perturbation analysis of neural collapse. *arXiv preprint arXiv:2210.16658*, 2022.
- Trivedi, S., Wang, J., Kpotufe, S., and Shakhnarovich, G. A consistent estimator of the expected gradient outerproduct. In *UAI*, pp. 819–828, 2014.
- Wang, P., Liu, H., Yaras, C., Balzano, L., and Qu, Q. Linear convergence analysis of neural collapse with unconstrained features. In *OPT 2022: Optimization for Machine Learning (NeurIPS 2022 Workshop)*, 2022.
- Wang, Z., Luo, Y., Zheng, L., Huang, Z., and Baktashmotlagh, M. How far pre-trained models are from neural collapse on the target dataset informs their transferability. In *Proceedings of the IEEE/CVF International Conference on Computer Vision*, pp. 5549–5558, 2023.
- Weinan, E. and Wojtowytsch, S. On the emergence of simplex symmetry in the final and penultimate layers of neural network classifiers. In *Mathematical and Scientific Machine Learning*, 2022.
- Woodbury, M. A. *Inverting modified matrices*. Department of Statistics, Princeton University, 1950.
- Xu, M., Rangamani, A., Liao, Q., Galanti, T., and Poggio, T. Dynamics in deep classifiers trained with the square loss: Normalization, low rank, neural collapse, and generalization bounds. In *Research*, volume 6, 2023.
- Yuan, G., Xu, M., Kpotufe, S., and Hsu, D. Efficient estimation of the central mean subspace via smoothed gradient outer products. *arXiv preprint arXiv:2312.15469*, 2023.
- Zhou, J., Li, X., Ding, T., You, C., Qu, Q., and Zhu, Z. On the optimization landscape of neural collapse under mse loss: Global optimality with unconstrained features. In *International Conference on Machine Learning (ICML)*, 2022.
- Zhu, L., Liu, C., Radhakrishnan, A., and Belkin, M. Catalysts in sgd: spikes in the training loss and their impact on generalization through feature learning. *arXiv preprint arXiv:2306.04815*, 2023.

## A. Proofs

**Proposition 5.1.** *Let  $x, y \in \mathbb{R}^d$  be two fixed vectors of unit length. Let  $W \in \mathbb{R}^{D \times d}$  be a weight matrix whose entries are initialized i.i.d. from  $\mathcal{N}(0, 2/D)$ . Assume  $x^\top y = r$ . Then,*

$$\begin{aligned} \mathbb{E}(\sigma(Wx)^\top \sigma(Wy)) &= \frac{(1-r^2)^{3/2}}{\pi} + \frac{r^2 \sqrt{1-r^2}}{\pi} \\ &+ \frac{r}{2} + \frac{r}{\pi} \arctan\left(\frac{r}{\sqrt{1-r^2}}\right). \end{aligned} \quad (1)$$

Moreover, the variance of this dot product scales with  $1/D$ , and the product is sub-exponential, making it well-concentrated.

*Proof.* It can easily be seen that the separate indices  $(Wx, Wy)_{i=1}^D$  are i.i.d., therefore it suffices to analyze the  $\mathbb{E}(\sigma(w^\top x)\sigma(w^\top y))$  for a single row of  $W$ . For simplicity of computation, we will re-scale the  $w$  to have variance 1 entries and later re-scale back again. From the spherical symmetry of the multivariate standard normal distribution, we can without loss of generality assume that  $x = e_1 = (1, 0, \dots, 0)$  and  $y = re_1 + \sqrt{1-r^2}e_2 = (r, \sqrt{1-r^2}, 0, \dots, 0)$ . With this, the expectation reduces to  $\mathbb{E}(\sigma(w_1)\sigma(rw_1 + \sqrt{1-r^2}w_2))$ . We can further compute (while renaming  $x \equiv w_1; y \equiv w_2$ ):

$$\begin{aligned} \mathbb{E}(\sigma(w_1)\sigma(rw_1 + \sqrt{1-r^2}w_2)) &= \int_{\mathbb{R}} \int_{\mathbb{R}} \sigma(x)\sigma(rx + \sqrt{1-r^2}y) \frac{1}{2\pi} e^{-\frac{x^2}{2}} e^{-\frac{y^2}{2}} dx dy = \\ &\sqrt{1-r^2} \int_{\mathbb{R}} \sigma(x) \frac{1}{\sqrt{2\pi}} e^{-\frac{x^2}{2}} \left( \int_{\mathbb{R}} \sigma\left(\frac{r}{\sqrt{1-r^2}}x + y\right) \frac{1}{\sqrt{2\pi}} e^{-\frac{y^2}{2}} dy \right) dx \end{aligned}$$

For the inner-integral, denote  $a = \frac{r}{\sqrt{1-r^2}}x$  for now. Then the inner integral can be computed as:

$$\int_{-a}^{\infty} (y+a) \frac{1}{\sqrt{2\pi}} e^{-\frac{y^2}{2}} dy = \int_{-a}^{\infty} y \frac{1}{\sqrt{2\pi}} e^{-\frac{y^2}{2}} dy + a \int_{-a}^{\infty} \frac{1}{\sqrt{2\pi}} e^{-\frac{y^2}{2}} dy = \frac{1}{\sqrt{2\pi}} e^{-\frac{a^2}{2}} + a\Phi(a),$$

where  $\phi(\cdot), \Phi(\cdot)$  will denote the pdf and cdf of the standard normal, respectively. Plugging back into the outer integral we get:

$$(\dots) = \sqrt{1-r^2} \int_0^{\infty} \frac{x}{2\pi} e^{-\frac{x^2}{2(1-r^2)}} dx + r \int_0^{\infty} \frac{x^2}{\sqrt{2\pi}} e^{-\frac{x^2}{2}} \Phi\left(\frac{rx}{\sqrt{1-r^2}}\right) dx.$$

We will compute the two summands separately:

$$\int_0^{\infty} \frac{x}{2\pi} e^{-\frac{x^2}{2(1-r^2)}} dx = \frac{\sqrt{1-r^2}}{\sqrt{2\pi}} \int_0^{\infty} \frac{x}{\sqrt{1-r^2}\sqrt{2\pi}} e^{-\frac{x^2}{2(1-r^2)}} dx = \frac{1-r^2}{2\pi},$$

where the last equality is a well-known formula for the expectation of ReLU of a Gaussian. For the second integral, denote  $a = \frac{r}{\sqrt{1-r^2}}$  and, using the integration by parts for  $x\phi(x)$  and  $x\Phi(ax)$  we can write

$$\begin{aligned} \int_0^{\infty} x^2 \phi(x) \Phi(ax) dx &= [-x\phi(x)\Phi(ax)]_0^{\infty} + \int_0^{\infty} \phi(x)\Phi(ax) dx + a \int_0^{\infty} x\phi(x)\phi(ax) dx \\ &= \int_0^{\infty} \phi(x)\Phi(ax) dx + a \int_0^{\infty} x\phi(x)\phi(ax) dx. \end{aligned}$$

The second integral evaluates to the same expression as the integral in the first summand above, but gets multiplied by  $a$  and thus equals  $\frac{r\sqrt{1-r^2}}{2\pi}$ . For the second integral, first note that this parametric integral is differentiable w.r.t.  $a$  and satisfies the condition on exchanging the derivative with the integral, so we will compute it using differentiation w.r.t.  $a$ . The value of the integral for  $a = 0$  is trivially  $1/4$ . After taking the derivative, it is easy to see that the integral evaluates to the same one we already computed twice, so denoting  $f(a) = \int_0^{\infty} \phi(x)\Phi(ax) dx$  we get

$$f'(a) = \frac{1}{2\pi(1+a^2)}.$$

We see that the  $f'$  is just half of the pdf of standard Cauchy distribution, while  $f(0)$  is half of its cdf, therefore  $f$  is half of its cdf and we can write:

$$f(a) = \frac{1}{4} + \frac{1}{2\pi} \arctan(a).$$

Plugging back the  $a$  and putting everything together we get the final:

$$\mathbb{E}(\sigma(w_1)\sigma(rw_1 + \sqrt{1-r^2}w_2)) = \frac{(1-r^2)^{\frac{3}{2}}}{2\pi} + \frac{r^2\sqrt{1-r^2}}{2\pi} + \frac{r}{4} + \frac{r}{2\pi} \arctan\left(\frac{r}{\sqrt{1-r^2}}\right).$$

We see that after scaling the weights with the scaling indicated in the statement, we get the final result. Since  $\sigma(w^T x)^T \sigma(w^T y)$  is clearly sub-exponential, the sum of  $D$  such i.i.d. variables will be as well.  $\square$

### A.1. Non-asymptotic results

**Theorem 5.5.** *The optimal limiting solution of the Problem 4 is  $k^* = I_2 \otimes (\mathbf{1}_n \mathbf{1}_n^\top) = \frac{1}{2}(yy^\top + \mathbf{1}_{2n} \mathbf{1}_{2n}^\top)$ . Any positive definite  $k$  sufficiently close to this (positive semi-definite) solution is therefore nearly optimal.*

*Proof.* Denote  $\mathcal{L}(\alpha, k) = \alpha^T(k^2 + \mu k)\alpha - 2\alpha^T k y$ . If  $k$  is positive definite, we can compute the conditionally optimal  $\alpha^*|k$  explicitly by solving for the gradient equal to 0:

$$\nabla_\alpha \mathcal{L}(\alpha, k) = 2(k^2 + \mu k)\alpha - 2k y = 0 \iff \alpha = (k + \mu I)^{-1} y.$$

Plugging this back into the objective and simplifying, we get:

$$\max_k y^T (k + \mu I)^{-1} k y.$$

Let  $k = V S V^T$  be the eigenvalue decomposition of  $k$ . Then, using  $(k + \mu I)^{-1} k = V(S + \mu I)^{-1} V^T V S V^T$ , we can equivalently rewrite this objective to:

$$\sum_{i=1}^{2n} (y^T v_i)^2 \frac{\lambda_i}{\lambda_i + \mu}.$$

By continuity of the Problem 3 in both variables, we can without loss of generality plug in  $k^*$  into this despite being low-rank. This can be seen by contradiction – if the  $\mathcal{L}(\alpha^*, k^*)$  would not be equal to the  $y^T (k + \mu I)^{-1} k y$ , we can find a converging sequence  $k_i$  of symmetric PD kernel matrices that converge to  $k^*$  for which the two objectives are equal and by continuity they converge to the objectives evaluated at  $\alpha^*, k^*$ , thus they must be equal as well.

Therefore,  $\mathcal{L}(\alpha^*, k^*)$  evaluates to  $2n \frac{n}{n+\mu}$ . We show that any symmetric PD kernel  $k$  cannot achieve better objective value. Note that  $\sum_{i=1}^{2n} (y^T v_i)^2 = 2n$  since  $(v_i)_{i=1}^{2n}$  forms an orthogonal basis and therefore a tight frame with constant 1. Moreover,  $\sum_{i=1}^{2n} \lambda_i = 2n$ , since the diagonal entries of  $k$  are by definition all equal 1. After normalizing  $y$  to unit norm, looking back at Equation 5 we see that we have a weighted average of  $\lambda_i/(\lambda_i + \mu)$ , where the weights correspond to the the alignment between  $y$  and  $v_i$  - the corresponding eigenvector. We want  $y$  to be most aligned with the eigenvectors corresponding to the biggest eigenvalues. Note that this is the case for the  $k^*$ , where  $y^T v_i = 0$  for all  $i \geq 3$ , thus all eigenvectors of the zero eigenvalue and  $(y^T v_i)^2 = n$  for the leading two eigenvalues that are both equal  $n$ .

Beating the value of 5 with another  $k$  would require having at least one eigenvalue bigger than  $n$  (the leading one) and the corresponding alignment  $(y^T v_1)^2 \geq n$ . This can be seen by concavity of the function  $g(x) = \frac{x}{x+\mu}$ , since

$$\sum_{i=1}^{2n} \omega_i g(\lambda_i) \leq g\left(\sum_{i=1}^{2n} \omega_i \lambda_i\right) \leq g(\omega_1 \lambda_1 + (1 - \omega_1)(2n - \lambda_1)).$$

From the rightmost expression it is clear that  $\omega_1$  must be at least a half. However, this is impossible due to the Perron-Frobenius theorem, which states that a positive matrix has a simple leading eigenvalue with strictly positive eigenvector, therefore  $(y^T v_1) < n$  since  $v_1$  is entry-wise positive.  $\square$

## A.2. Asymptotic results

**Lemma A.1** (Woodbury Inverse Formula (Woodbury, 1950)).

$$(P + UV^\top)^{-1} = P^{-1} - P^{-1}U(I + V^\top P^{-1}U)^{-1}V^\top P^{-1}.$$

**Lemma A.2** (Fixed point of collapse). *Let  $A^* = yy^\top + \lambda_\Phi I$ , the collapsed data gram matrix following an application of the non-linear random feature map  $\Phi$ . Then,*

$$(A^*)^{-1} = \lambda_\Phi^{-1}I - \lambda_\Phi^{-1}(\lambda_\Phi + n)^{-1}yy^\top.$$

*Proof of Lemma A.2.* We write  $yy^\top = nUU^\top$ , where  $U \in \mathbb{R}^{n \times K}$  is the matrix of normalized eigenvectors of  $yy^\top$ . By Lemma A.1 and that  $U^\top U = I$ ,

$$\begin{aligned} (A^*)^{-1} &= (\lambda_\Phi I + nUU^\top)^{-1} \\ &= \lambda_\Phi^{-1}I - \frac{n}{\lambda_\Phi^2}U(I + n\lambda_\Phi^{-1}U^\top U)^{-1}U^\top \\ &= \lambda_\Phi^{-1}I - \frac{n}{\lambda_\Phi^2} \cdot \frac{1}{1 + n\lambda_\Phi^{-1}}UU^\top \\ &= \lambda_\Phi^{-1}I - \frac{n}{\lambda_\Phi(\lambda_\Phi + n)}UU^\top \\ &= \lambda_\Phi^{-1}I - \frac{\lambda_\Phi^{-1}}{\lambda_\Phi + n}yy^\top. \end{aligned}$$

□

*Proof of Proposition 5.4.* We have solved the kernel ridgeless regression problem to get coefficients  $\alpha = (X_l X_l^\top + \lambda_k I)^{-1}y$ . Then, the predictor at layer  $l$  evaluated on the training data is,

$$f_l(X_l) = (X_l^\top X_l + \lambda_k I)\alpha.$$

As in Deep RFM, let  $M$  be the AGOP. Then,

$$M = \sum_{i=1}^n \nabla f(x^{(i)})(\nabla f(x^{(i)}))^\top = X_l \alpha \alpha^\top X_l^\top.$$

We drop the subscript  $l$  for simplicity. Therefore,

$$X^\top M X = X^\top X (X^\top X + \lambda_k I)^{-1} yy^\top (X^\top X + \lambda_k I)^{-1} X^\top X.$$

Let  $A = X^\top X$ . Applying Lemma A.1,

$$(A + \lambda_k I)^{-1} = A^{-1} - \lambda_k A^{-1} (I + \lambda_k A^{-1})^{-1} A^{-1}.$$

Therefore,

$$X^\top M X = \left( I - \lambda_k (I + \lambda_k A^{-1})^{-1} A^{-1} \right) yy^\top \left( I - \lambda_k (I + \lambda_k A^{-1})^{-1} A^{-1} \right).$$

Applying that, by assumption,  $\lambda_k \lambda_\Phi^{-1}$  is a small value  $\epsilon_{\text{lin}}$ , and as  $\lambda_\Phi$  is the minimum eigenvalue of  $A$ , we have that  $\lambda_k \|A^{-1}\| \leq \lambda_k \lambda_\Phi^{-1} \triangleq \epsilon_{\text{lin}}$ . Therefore,  $(I + \lambda_k A^{-1})^{-1} \lambda_k A^{-1} = \lambda_k A^{-1} - (\lambda_k A^{-1})^2 + \dots = \lambda_k A^{-1} + O(\epsilon_{\text{lin}}^2)$ , where  $O(\epsilon_{\text{lin}}^2)$  refers to some matrix of spectral norm at most  $C\epsilon_{\text{lin}}^2$  for some constant  $C > 0$ . Then,

$$X^\top M X = (I - \lambda_k A^{-1} + O(\epsilon_{\text{lin}}^2)) yy^\top (I - \lambda_k A^{-1} + O(\epsilon_{\text{lin}}^2)) = yy^\top - \lambda_k A^{-1} yy^\top - \lambda_k yy^\top A^{-1} + O(\epsilon_{\text{lin}}^2).$$

Let  $\tilde{A} = \frac{A-A^*}{\|A-A^*\|}$ , and  $\epsilon_A = \|A - A^*\|$ . Then, applying Lemma A.1,

$$A^{-1} = \left( A^* + \epsilon_A \tilde{A} \right)^{-1} = \left( I + \epsilon_A (A^*)^{-1} \tilde{A} \right)^{-1} (A^*)^{-1} = (A^*)^{-1} - \epsilon_A (A^*)^{-1} \left( I + \epsilon_A \tilde{A} (A^*)^{-1} \right)^{-1} \tilde{A} (A^*)^{-1} .$$

Let  $\tilde{\Psi} = \left( I + \epsilon_A \tilde{A} (A^*)^{-1} \right)^{-1}$ . Assuming partial collapse has already occurred, i.e.,  $\epsilon_A \lambda_{\Phi}^{-1} < 1/2$ ,

$$\|\tilde{\Psi}\| \leq (1 - \epsilon_A \lambda_{\Phi}^{-1})^{-1} \leq 2 .$$

In this case, using that  $yy^\top (A^*)^{-1} = (A^*)^{-1} yy^\top = (1 + \lambda_{\Phi}^{-1}) yy^\top$  (Lemma A.2),

$$\begin{aligned} X^\top MX &= yy^\top - \lambda_k A^{-1} yy^\top - \lambda_k yy^\top A^{-1} + O(\epsilon_{\text{lin}}^2) \\ &= yy^\top - \lambda_k (A^*)^{-1} yy^\top - \lambda_k yy^\top (A^*)^{-1} + O(\epsilon_{\text{lin}}^2) \\ &\quad - \lambda_k \epsilon_A (A^*)^{-1} \tilde{\Psi} \tilde{A} (A^*)^{-1} yy^\top - \lambda_k \epsilon_A yy^\top (A^*)^{-1} \tilde{A} \tilde{\Psi} (A^*)^{-1} \\ &= yy^\top - 2\lambda_k (1 + \lambda_{\Phi}^{-1}) yy^\top + O(\epsilon_{\text{lin}}^2) \\ &\quad - \lambda_k \epsilon_A (1 + \lambda_{\Phi}^{-1}) (A^*)^{-1} \tilde{\Psi} \tilde{A} yy^\top - \lambda_k \epsilon_A (1 + \lambda_{\Phi}^{-1}) yy^\top \tilde{A} \tilde{\Psi} (A^*)^{-1} . \end{aligned}$$

Therefore, where  $\kappa = 1 - 2\lambda_k (1 + \lambda_{\Phi}^{-1}) > 1/2$  by choice of  $\lambda_k \cdot 2\lambda_{\Phi}^{-1} (1 + \lambda_{\Phi}^{-1}) n < 1 - \epsilon$ ,

$$\begin{aligned} \|X_{l+1}^\top X_{l+1} - A^*\| &= \|\kappa^{-1} X^\top MX - yy^\top\| \\ &= \left\| O(\epsilon_{\text{lin}}^2) + \epsilon_A \cdot \lambda_k \cdot 2\kappa^{-1} (1 + \lambda_{\Phi}^{-1}) (A^*)^{-1} \tilde{\Psi} \tilde{A} yy^\top \right\| \\ &\leq O(\epsilon_{\text{lin}}^2) + \epsilon_A \cdot \lambda_k \cdot 2\lambda_{\Phi}^{-1} (1 + \lambda_{\Phi}^{-1}) n \\ &< O(\epsilon_{\text{lin}}^2) + \epsilon_A (1 - \epsilon) \\ &= O(\epsilon_{\text{lin}}^2) + (1 - \epsilon) \|X_l X_l^\top - A^*\| . \end{aligned}$$

It remains to show that partial collapse,  $\epsilon_A \lambda_{\Phi}^{-1} < 1/2$ , happens in the first iteration. To ensure this condition, recall,

$$X^\top MX = yy^\top - \lambda_k A^{-1} yy^\top - \lambda_k yy^\top A^{-1} + O(\epsilon_{\text{lin}}^2) .$$

Therefore, because  $\|A^{-1}\| \leq \lambda_{\Phi}^{-1}$ , where  $\Psi$  is some error matrix with norm 1,

$$X^\top MX = yy^\top + \lambda_k \lambda_{\Phi}^{-1} n \Psi + O(\lambda_k^2 \lambda_{\Phi}^{-2}) .$$

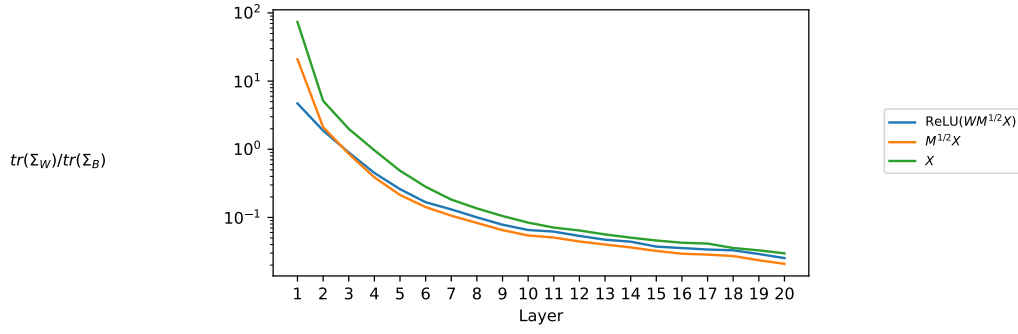
Therefore,

$$\|X^\top MX - yy^\top\| < 1/2 ,$$

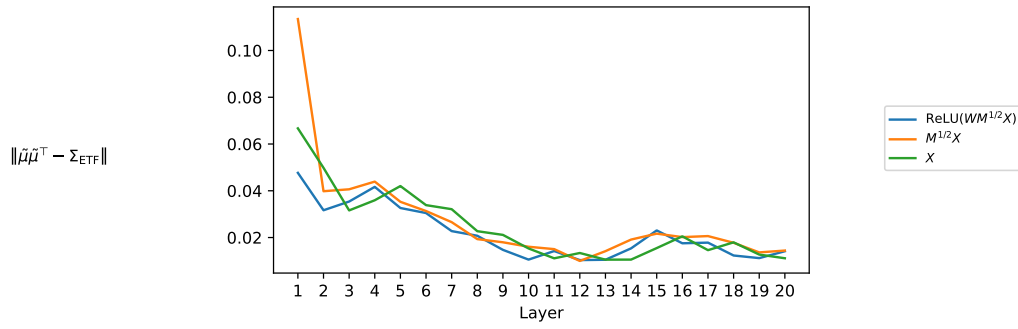
provided  $\lambda_k \lambda_{\Phi}^{-1} n < C_1/2$ , for some universal constant  $C_1$ . □

## B. Additional plots

### B.1. Deep RFM

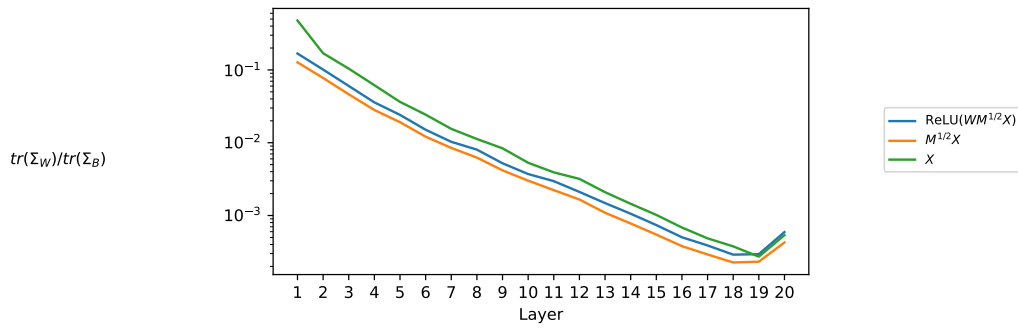


(a)  $\text{tr} \Sigma_W / \text{tr} \Sigma_B$ , our NC1 metric.

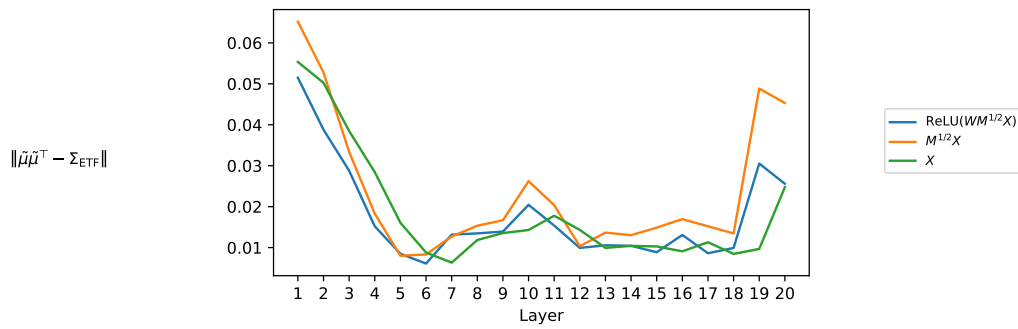


(b)  $\|\tilde{\mu}\tilde{\mu}^\top - \Sigma_{\text{ETF}}\|$ , our NC2 metric.

Figure 5. Neural collapse with Deep RFM on SVHN.



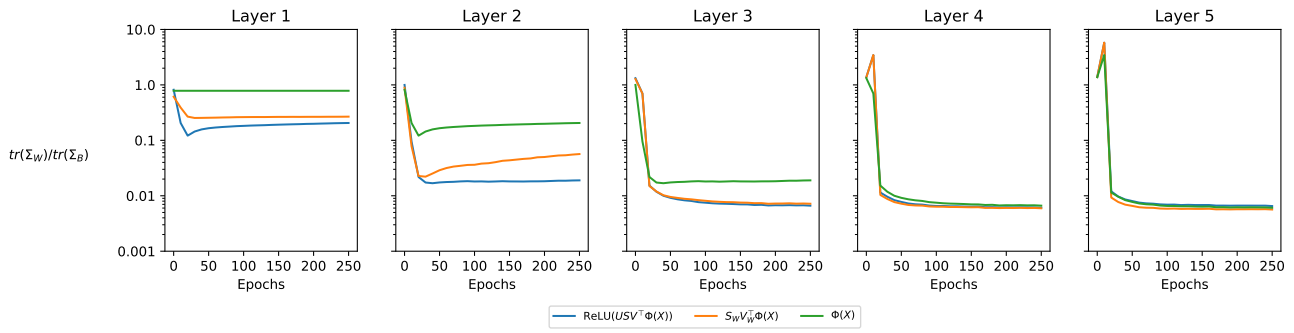
(a)  $\text{tr} \Sigma_W / \text{tr} \Sigma_B$ , our NC1 metric.



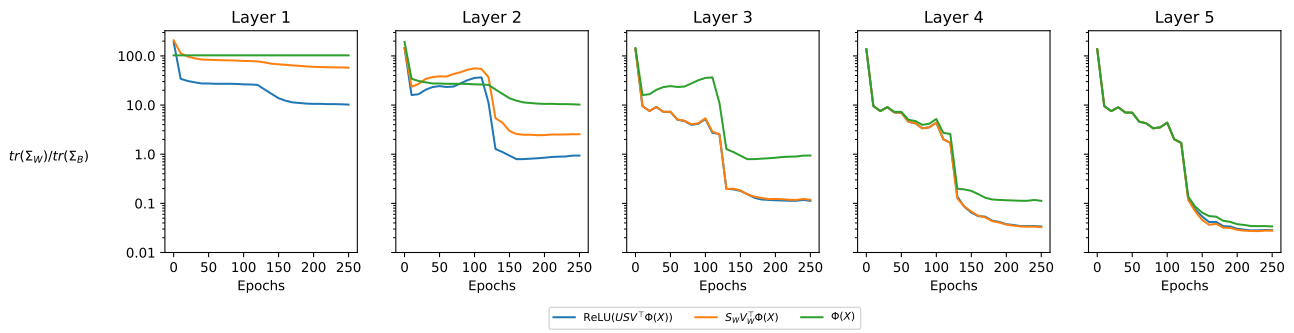
(b)  $\|\tilde{\mu}\tilde{\mu}^\top - \Sigma_{\text{ETF}}\|$ , our NC2 metric.

Figure 6. Neural collapse with Deep RFM on MNIST.

B.2. Neural networks



(a) MNIST.



(b) SVHN.

Figure 7. Feature variability collapse (NC1) from different singular value decomposition components.

## B.3. NFA metrics for neural networks

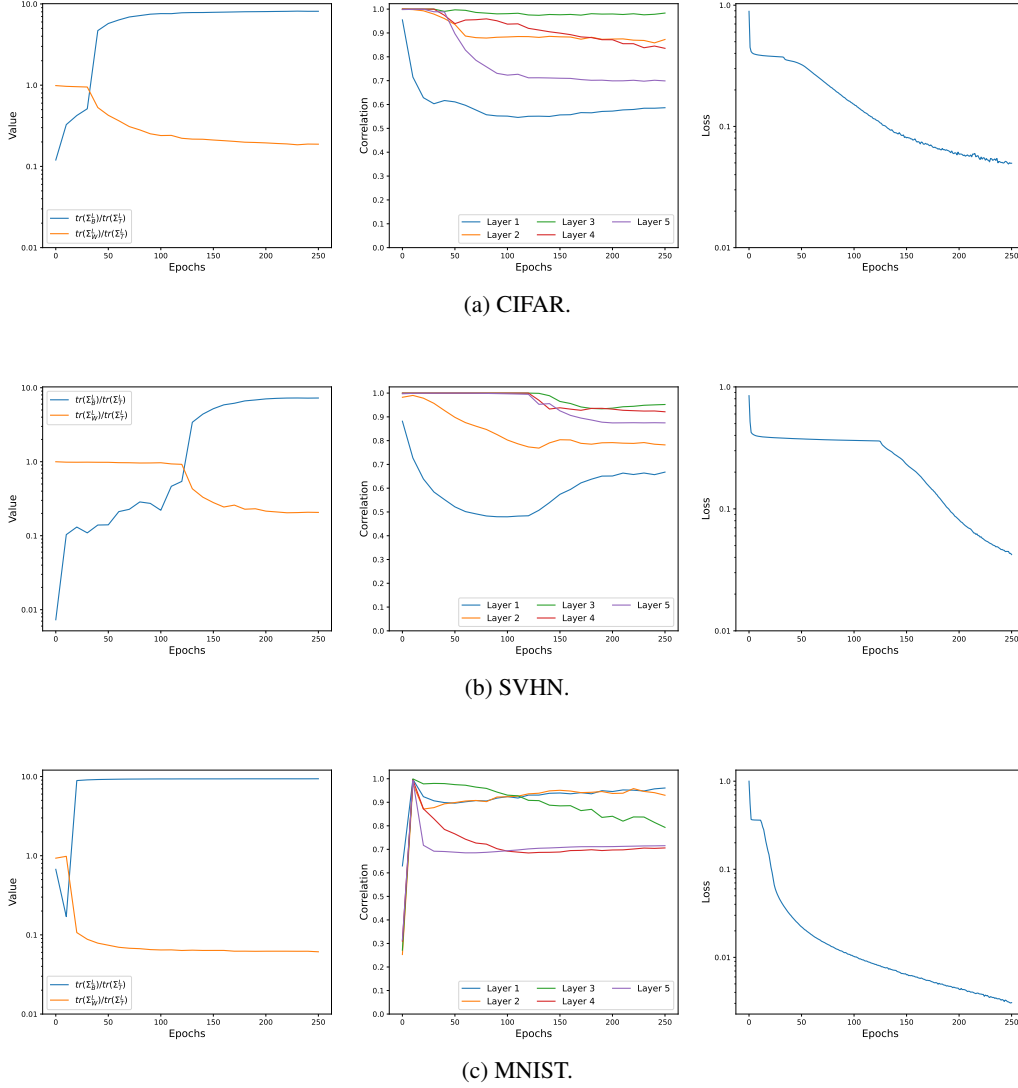


Figure 8. Train loss and NFA correlations. In the first column, we plot the evolution of  $\text{tr} \Sigma_W / \text{tr} \Sigma_T$  and  $\text{tr} \Sigma_B / \text{tr} \Sigma_T$ , where  $\Sigma_T \triangleq \Sigma_W + \Sigma_B$ . In the second column we plot the development of the NFA, where correlation is measured between  $W_l^T W_l$  and the square root of the AGOP with respect to the inputs at layer  $l$ ,  $X_l$ . The third column is the train loss of the neural network.

## C. Experimental details

In both Deep RFM and neural networks, we one hot encode labels and use  $\pm 1$  for within/outside of each class.

For the neural network experiments, we use 5 hidden layer MLP networks with no biases and ReLU activation function, initialized using Xavier Uniform with initialization scale 0.01 in all hidden layers. We use default initialization for the linear readout layer. The layers all use width 512. We train with Adam using no weight decay and learning rate  $2 \times 10^{-5}$  for 250 epochs and measure the AGOP and NC metrics every 10 epochs.

For the Deep RFM experiments, we use the Laplace kernel  $k$ , which evaluates two datapoints  $x, z \in \mathbb{R}^d$  as  $k(x, z) = \exp(-\|x - z\|_2/L)$ , where  $L$  is a bandwidth parameter. In these experiments, we set  $L = 2.0$ . We perform ridgeless regression to interpolate the data, i.e.  $\mu = 0$ . We use width 512 for the random feature map in Deep RFM with ReLU activation function.

Unless otherwise specified, we perform experiments using the first 50,000 points from each of MNIST, SVHN, and CIFAR-10 loaded with Torchvision datasets.